Evolution of the crystal growth mechanism of zeolite W (MER) with temperature

Maarten Houlleberghs, Eric Breynaert, Karel Asselman, Ewoud Vaneeckhaute, Sambhu Radhakrishnan, Michael W Anderson, Francis Taulelle, Mohamed Haouas, Johan A Martens, Christine E.A. Kirschhock

Evolution of the crystal growth mechanism of zeolite W (MER) with temperature

Maarten Houlleberghs,[a,#] Eric Breynaert,[a,#,] Karel Asselman,[a] Ewoud Vaneeckhaute,[a] Sambhu Radhakrishnan,[a] Michael W. Anderson,[b] Francis Taulelle,[a,c] Mohamed Haouas,[c] Johan A. Martens[a] and Christine E.A. Kirschhock[a,*]*

[a] KU Leuven, Center for Surface Chemistry and Catalysis, Department of Microbial and Molecular Systems (M2S), Celestijnenlaan 200F, Box 2461, 3001 Leuven, Belgium.

[b] Centre for Nanoporous Materials, School of Chemistry, The University of Manchester, Oxford Road, Manchester M13 9PL, UK.

[c] Institut Lavoisier de Versailles, UVSQ, University of Paris-Saclay, 45 Avenue des Etats-Unis, 78035 Versailles Cedex, France.

[#]M.H. and E.B. contributed equally

*Corresponding authors: christine.kirschhock@kuleuven.be; eric.breynaert@kuleuven.be

Abstract

The morphology of zeolite W (MER topology) synthesized from *Hydrated Silicate Ionic Liquids* (HSILs) shows a distinct temperature dependence, reflected in a fundamental difference in the underlying crystal growth mechanism as revealed by Atomic Force Microscopy (AFM). Zeolite W crystals obtained at 90 °C develop in a highly supersaturated solution through *birth and spread* growth, whereas synthesis at 175 °C results in elongated, *spiral* grown zeolite W particles. Supersaturation was measured through the concentration of dissolved aluminate, being the limiting species. The evolution of the aluminum concentration during crystallization at different temperatures was monitored with ^{27}Al Nuclear Magnetic Resonance (NMR) spectroscopy. Supersaturation conditions determine the nucleation rate, the prevailing crystal growth mechanism, and resulting crystal morphology.

Keywords: merlinoite (MER); crystal growth mechanism; AFM; ^{27}Al NMR

1. Introduction

Nucleation and growth of zeolite crystals are complex processes and have been a topic of extensive research over de past decades [1]. Zeolite structures have long been considered as ordered compilations of secondary building units (SBUs). Zeolite SBUs are defined as arrangements of atoms represented by a graph, with tetrahedrally coordinated atoms (T-atoms) as nodes and siloxane bonds between them as links [2]. A recent development in crystal description is however the construction of the topology from tiles rather than graphs. As its main advantage the tiling representation offers a simple criterion for accepting an arrangement of building units as a valid crystal: crystals are compact tilings without any voids. This concept has led to the definition of natural building units (NBUs) [3]. NBUs represent a variety of polyhedra, ranging from large cage-like structures and channel segments to small units such as cubes and hexagonal prisms, which allow an unambiguous description of the crystal space [2, 3]. In contrast with SBUs, NBUs are sharing faces rather than corners. Each face of a unit is consequently shared between two tiles. Upon dissolution, the most fragile bonds in a structure are broken so that discrete units are removed from the surface. This implies dissolution does not involve a statistical removal of arbitrary "pieces", but rather the extraction of discrete well-defined species, so that the remaining surface ideally consists of closed tiles only [4, 5]. This process can be observed with 'contact-mode' Atomic Force Microscopy (AFM), revealing the relevance of NBUs in describing a zeolite crystal.

The potential of 'contact-mode' AFM for investigating the growth of zeolites was initially demonstrated by Brent *et al.* (2008) for zeolite L [6] and by Meza *et al.* (2007) for zeolite A [5]. Very recently, Anderson *et al.* (2017) extended this approach and combined the information on prevailing growth patterns and features on the crystal surface with other techniques to gain deeper insight in the crystal growth. This led to the construction of a model capable of accurately predicting the growth of a wide range of zeolite crystals. The option to simultaneously simulate crystal habit and surface topology provides an unprecedented tool to investigate crystallization [7].

Despite the wealth of information obtained from AFM, molecular understanding of zeolite growth can only be obtained by matching the crystal growth with the chemistry occurring in solution and at the crystal surface. Here, zeolite synthesis from *Hydrated Silicate Ionic Liquids* (HSILs), first reported by Taulelle's group (2014), offers valuable opportunities [8, 9]. The homogeneity of the HSIL and the absence of a gel phase enable identification of speciation in the liquid phase via liquid-state high resolution Nuclear Magnetic Resonance (NMR) spectroscopy, optical and X-ray scattering techniques as well as Electrochemical Impedance Spectroscopy (EIS) [8, 10-12]. This allows the characterization of crystal growth on a molecular scale and the investigation of less explored synthesis parameters such as zeolite solubility products and supersaturation conditions [13-15]. The absence of a gel phase also allows to quench syntheses at different points in time and to recover well-defined separate crystals next to the exact supernatant composition. Preparation of an HSIL entails the hydrolysis of tetraethyl orthosilicate (TEOS) in an aqueous KOH solution and removal of the upper water-ethanol layer after spontaneous phase separation [8]. Addition of aluminum as e.g. alkali-aluminate to the HSIL results in a clear, homogeneous synthesis

mixture yielding various zeolite frameworks, among them extra-large zeolite W crystals depending on the composition of the precursor mixture, temperature and time [8, 9]. HSIL based synthesis, similar to zeolite transformation in inorganic media [16, 17], precludes the need for organic structure directing agents (SDAs), which asides the absence of a gel phase is a further asset of this method.

Zeolite W[§] (framework code MER), also referred to as synthetic merlinoite, is a small-pore zeolite with a channel system consisting of three-dimensional, interconnected 8-membered ring (8MR) pores[§§] as illustrated in Figure 1 [18, 19]. Natural merlinoite was first discovered in 1977 in the cracks of a mineral deposit near Rieti, Italy [20]. Surprisingly, its synthetic counterpart had already been synthesized by Breck in 1953 and was designated zeolite W [21-23].

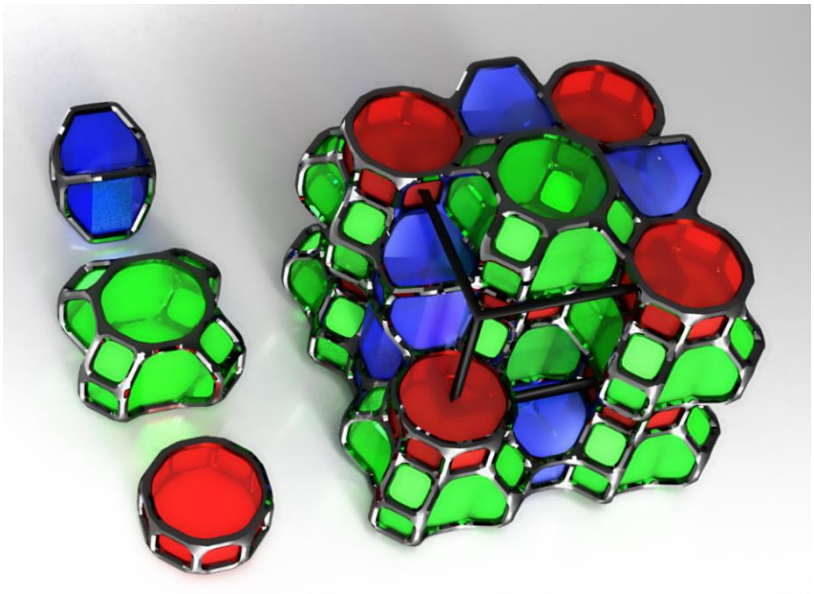

Figure 1. The MER framework structure of zeolite W can be assembled from three natural tiles: t-opr (red), t-pau (green) and t-ste (blue).

Zeolite W (Figure 1) has hitherto remained absent from crystal growth studies, most likely because of its typically small crystal size and the heavily aggregated nature of available synthetic samples. However, large MER crystals can be obtained using HSILs and allow the detailed study of habit and mechanism of growth [8].

2. Experimental

In this work, large zeolite W crystals were grown from a 0.5 SiO_2 : 0.013 Al_2O_3 : 1 KOH : 8 H_2O synthesis mixture which was prepared according to the procedure described by Haouas *et al.* (2014) [8]. The synthesis mixture was transferred to a Teflon-lined stainless steel autoclave and heated at 90, 150 and 175 °C for 48 hours in a tumbling oven. The recovered solid phase was characterized with X-ray Diffraction (XRD), ^{27}Al solid state Nuclear Magnetic Resonance (NMR) spectroscopy, Scanning Electron Microscopy (SEM) and Atomic Force Microscopy (AFM). The corresponding supernatants were analyzed with ^{27}Al liquid state NMR.

X-ray diffraction patterns were recorded on a STOE STADI P Combi diffractometer with focusing Ge(111) monochromator ($CuK_{\alpha 1}$ radiation, λ = 0.154 nm) with high throughput set-up in transmission geometry and with 140°-curved image plate position sensitive detector (IP PSD) from 0 to 62.5° 2 θ.

Solid-state MAS NMR investigation into the molecular structure of the zeolite W samples was performed at 298 K (BCU II) using a standard bore Bruker AVANCE III HD spectrometer with a H/X CP-MAS probe operating at 300.13 MHz for ^{1}H and 78.172 MHz for ^{27}Al. Data collection was performed at spinning speeds of 14 kHz, using a π/12 flip angle, a repetition delay of 2 s and chemical shift referencing with respect to a 0.5 M aluminum

nitrate solution at 0 ppm. Proton decoupling was performed during acquisition with spinal64 [24].

High-resolution SEM was performed on a Nova NanoSEM 450 (FEI Eindhoven). Powder samples were dispersed on carbon tape attached to aluminum stubs and imaged without any further sample modification. High-resolution images were obtained at low voltages (2 kV) using a Centered Back Scattering detector (CBS, a new type of BSE detector) combined with Beam Deceleration Mode.

'Contact-mode' AFM was carried out on a JPK Nanowizard II Bio-AFM mounted on an inverted Axiovert 200 MAT optical microscope. Samples were prepared by heating a small fragment of thermoplastic resin on a glass slide at 50 °C for 1.5 minutes. A small amount of sample was then dispersed on the softened resin and re-heated at 50 °C for an additional minute to firmly fix the sample in the thermoplast. Finally, excess sample was removed using compressed air. Silicon nitride tips (Bruker probes NP-10, spring constant 0.58 Nm^{-1}) were used with a scan rate of 1-2 Hz. Images were analyzed using the JPK Data Processing software.

Analysis of the supernatant solutions was carried out on a Bruker Avance 500 spectrometer, operating at 130.326 MHz for ^{27}Al. In a modified background-free probe, 10 mm PTFE tubes were used to avoid the strong background signal of glass and quartz tubes. The ^{27}Al NMR spectra were obtained by applying 2.14 µs ($\pi/12$) pulses, a recycle delay of 0.1 s, an acquisition time of 26 ms and accumulating 1024 scans. The chemical shifts were determined with respect to an aqueous solution (0.7 $mol.L^{-1}$) of $Al(NO_3)_3$. NMR

quantification was performed by spectral decomposition analysis. Simulation of all lines was conducted by using NMR notebook software program with Lorenzian shape.

3. Results and discussion

The zeolite W crystals recovered after 48 hours of aging exhibit a distinctive elongation of the morphology with increasing temperature, as revealed by SEM (Figure 2).

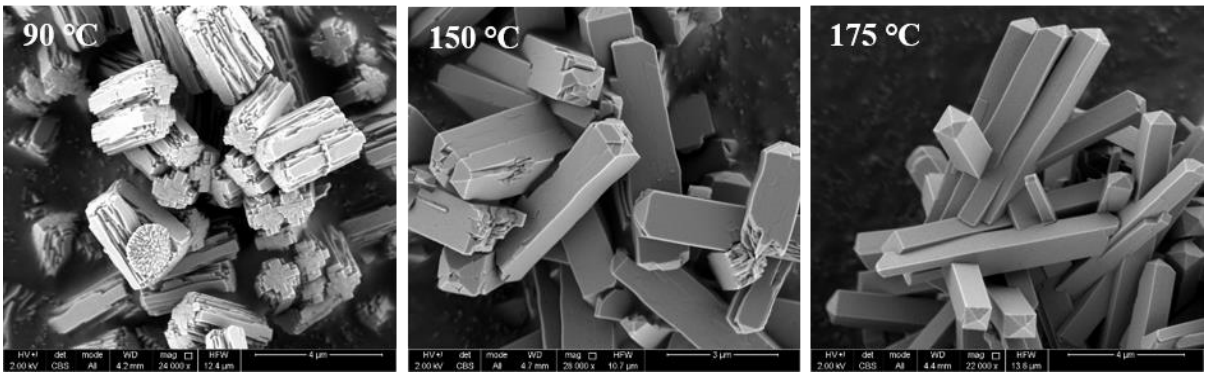

Figure 2. SEM images (Nova NanoSEM 450) of the solid products recovered from the 0.5 SiO_2 : 0.013 Al_2O_3 : 1 KOH : 8 H_2O precursor mixture after 48 hours of synthesis at 90, 150 and 175 °C. As temperature increases, the MER crystals become increasingly more elongated.

The change in morphology is not reflected on molecular level, as indicated by the ^{27}Al direct excitation MAS NMR spectra and X-ray diffraction patterns of the crystals as function of temperature (Figure 3). AFM characterization of their surface however revealed a fundamentally different crystal growth mechanism between samples obtained at 90 and 175 °C (Figure 4). Synthesis at 90 °C favors the formation of zeolite W through 'birth and spread' growth, whereas higher temperatures result in a spiral growth mechanism. 'Birth and spread' and spiral growth mechanisms are typically observed for crystals grown in high and

low supersaturation conditions, respectively. In the case of 'birth and spread' growth, the 2D nucleation rate is high, so that a new terrace is started before an entire layer is completed. Consequently, a terraced surface resembling the one shown in Figure 4a is obtained [25, 26].

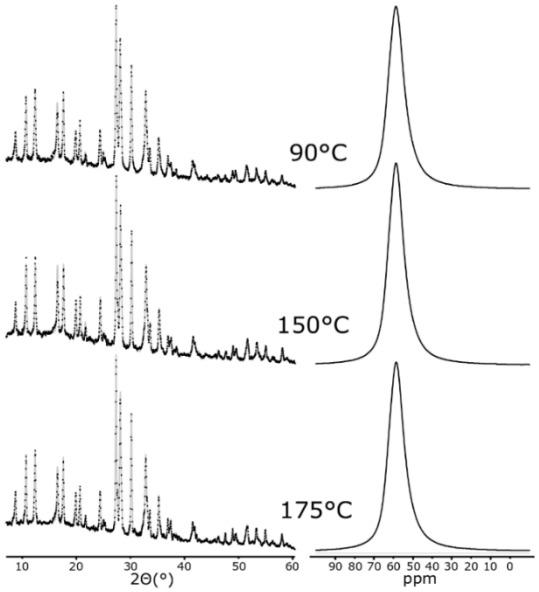

Figure 3. X-ray diffraction patterns (left) and ^{27}Al MAS NMR spectra (right) of zeolite W crystals obtained after 48 hours of synthesis at different temperatures. the diffraction patterns are fitted with the typical MER space group *Immm*, resulting in unit cell parameters between a = 14.16 Å and 14.23 Å, b = 13.99 Å and 14.055 Å, c = 10.02 Å and 10.05 Å.

For crystallization processes, supersaturation can generally be defined as the difference between the actual concentration of a solute, its ion activity product (IAP) and the equilibrium concentration or solubility of the solute at a given temperature [28]. All syntheses in this work were HSIL based, and could be quenched at different points in time to separate the homogeneous supernatant solution from the crystals to determine the speciation of its components. As only a few crystals were formed and the potassium based HSILs contained a limited fraction of Al, the concentration of potassium and silicon could

be considered constant throughout the synthesis. Consequently, supersaturation conditions could be directly derived from the monitored concentration of dissolved aluminate species.

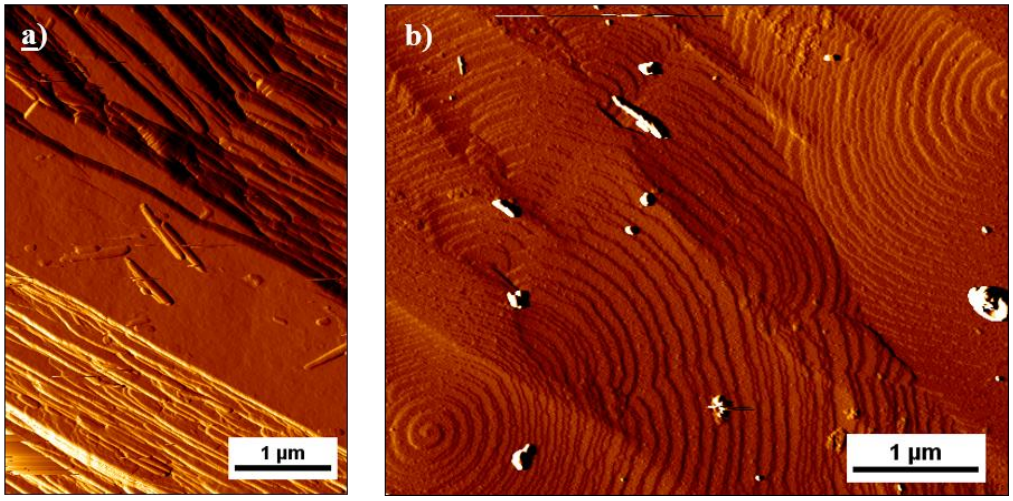

Figure 4. 'Contact-mode' AFM image (JPK Nanowizard II Bio-AFM) of the a) layered surface of a MER sample synthesized at 90 °C, indicating a 'birth and spread' growth mechanism; and b) (double) spiral surface patterns obtained at 175 °C which are specific for spiral growth [27].

Liquid state ^{27}Al NMR was used to analyze the supernatant solutions collected from syntheses quenched after 2, 4, 8, 16, 32 and 48 hours of synthesis (Figure 5). As sampling of the supernatant occurred after the reaction mixtures were allowed to cool to room temperature (RT, 23 °C), supersaturation is determined with respect to the solubility of the aluminate species at 23 °C (Figure 5).

The consumption of aluminate species appears to follow an S-shaped curve, typically observed in zeolite crystallization. The study was extended to include two intermediate temperatures (110 and 130 °C) to further evidence such behavior and to allow a detailed kinetic analysis of the formation process (see Supporting Information). Using the Avrami

equation [29], the activation energy (E_a) for crystallization of zeolite W in the HSIL based growth medium was estimated to be 47 ± 2 kJ/mol.

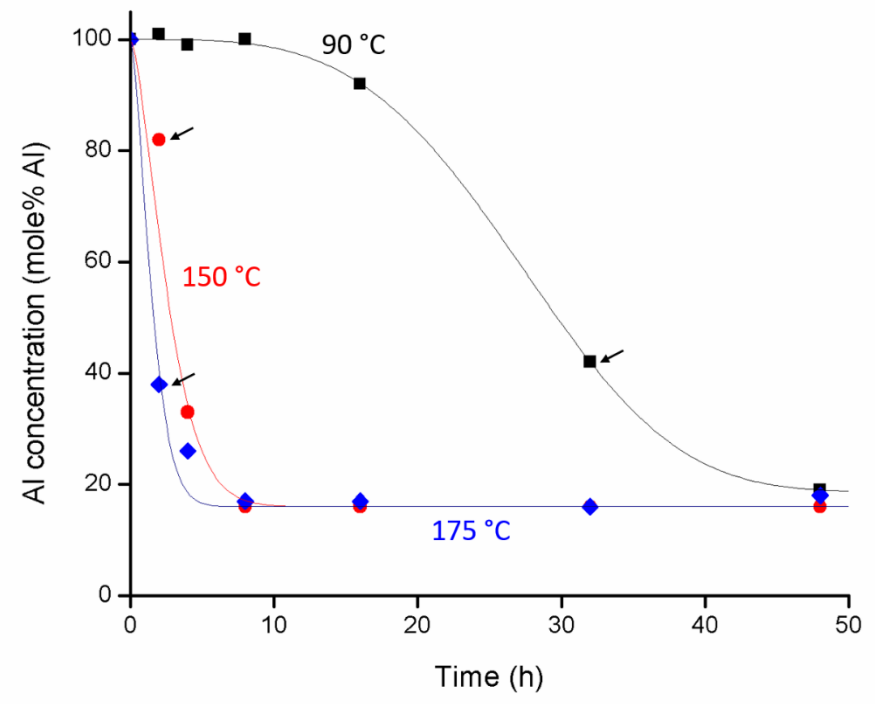

Figure 5. Evolution of the aluminum concentration in the supernatant after 2, 4, 8, 16, 32 and 48 hours of synthesis at 90 (black), 150 (red) and 175 °C (blue curve). The arrows mark the first appearance of solid crystallization products. All curves converge around 16 ± 3 mole%, indicating the solubility of zeolite W. Concentrations are expressed as percentages of the initial aluminate concentration (= 100%).

At the start of all syntheses, supersaturation is high, independent of the synthesis temperature. In these conditions, crystallization theory dictates that nucleation prevails. For the synthesis at 90°C, however (black curve, Figure 5), the thermal energy provided by the system appears to be too low to easily overcome the energetic barrier associated with 3D nucleation. Nucleation thus proceeds at a very slow rate and no significant change in

dissolved aluminum concentration is observed for 10 hours. Only after 16 hours, the aluminum content of the supernatant solution has decreased significantly, indicating an appreciable amount of stable nuclei has been formed and crystal growth has set in. Crystallization then proceeds at elevated rates and the aluminum concentration diminishes until solubility of the formed product is reached. This effect is similar to seeding, where addition of seed crystals to the synthesis mixture greatly improves the crystallization rate, as the nucleation step is omitted [30].

At 175 °C however, the system provides sufficient thermal energy to overcome the activation energy for nucleation and stable nuclei are rapidly and extensively formed. This results in low supersaturation conditions leading to domination of spiral growth, which at these conditions is faster than 2D nucleation of a new terrace (Figure 4b) [25, 31]. This particular growth mechanism is believed to initiate at screw dislocations: line defects in the crystal structure that result in the formation of a step on the crystal surface, making the need for 2D nucleation obsolete [32].

Zeolite formation is, similar to other crystallization processes, governed by the equilibrium between nucleation and growth. Supersaturation conditions typically determine nucleation rate and prevailing growth mechanism [28]. As zeolites are Q^4 silicates, typically forming in highly alkaline conditions, the final step in the assembly of a zeolitic precursor or zeolite framework requires the conversion of pairs of SiO^- groups in solution-born oligomers into Si-O-Si bridges on the precursor, nuclei, or crystal surface. As the activation energy for this condensation is high, zeolite synthesis is mostly limited to high temperatures and has long been considered special. Partial isomorphic substitution of Si with Al assists nucleation and growth as the formation of Si-O-Al bridges from SiO^- + $AlOH^-$ has a much lower

activation energy as compared to the less favorable $SiO^- + SiO^-$ pathway [9, 33]. Scheme 1 presents an overview of the reaction pathways discussed above**.**

Scheme 1. Reaction pathways leading to the formation of (alumino)silicate nano-aggregates

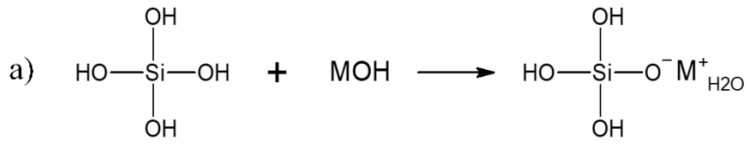

► Deprotonation of silicic acid in highly alkaline medium (pH = ± 13)

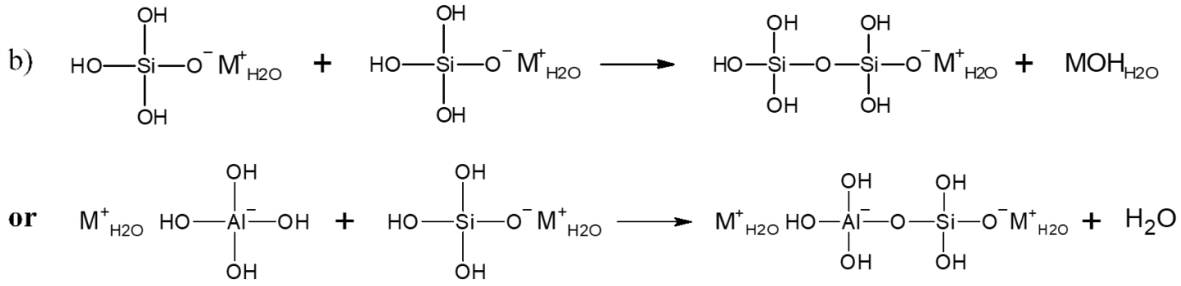

► Di- and oligomerization of tetrahedral building units into (alumino)silicate nano-aggregates through condensation by oxolation

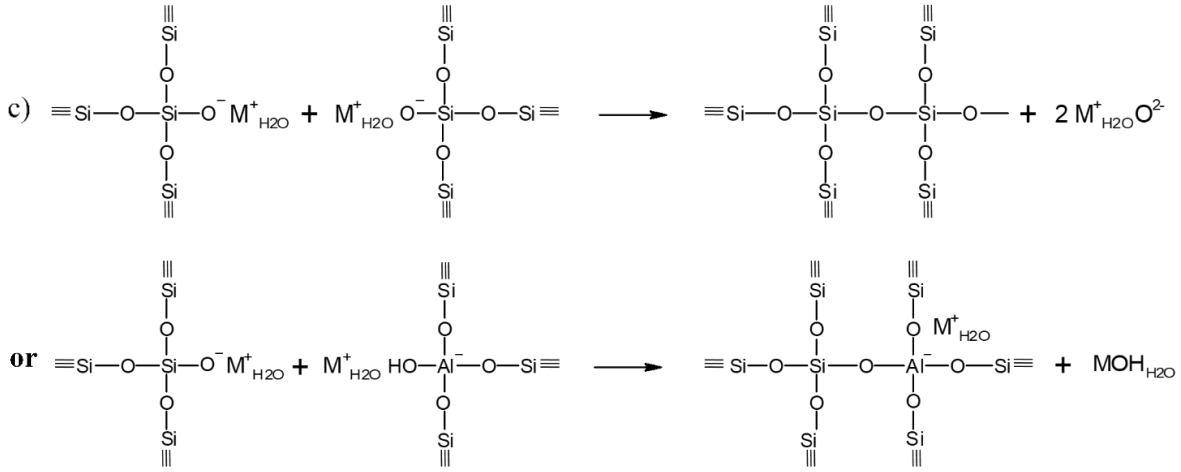

► Formation of Si-O-Si or Si-O-Al bridges between nano-aggregates through condensation; the latter forms preferentially due to its lower activation energy

Considering the evolution of the dissolved Al concentration during the synthesis in combination with the reactions in Scheme 1, it becomes evident that the yield of the synthesis of zeolite W from K based HSIL precursors is limited by the availability of Al and the synthesis kinetics is dependent on the synthesis temperature.

4. Conclusion

In this work, large zeolite W crystals (MER topology) were synthesized at different temperatures following a novel zeolite synthesis procedure based on the use of *Hydrated Silicate Ionic Liquids* (HSILs) as silicon source. Although the final yield appeared to depend almost exclusively on the overall Al concentration, growth mechanism and crystal morphology of the zeolite W crystals were shown to depend on the synthesis temperature. 'Contact-mode' Atomic Force Microscopy (AFM) revealed that samples grown at 90 °C develop through 'birth and spread' growth, whereas synthesis at 175 °C resulted in spiral grown zeolite W crystallites. The higher the temperature, the more elongated the crystal shape. Contrary to similar studies [34], supersaturation conditions were not 'deduced' but were qualitatively determined through speciation of the aluminate species in the supernatant solutions by ^{27}Al NMR, providing quantifiable thermodynamic evidence for the observed morphological transformation and differing growth mechanism: high supersaturation during crystal growth initiation at 90 °C resulted in a characteristic 'birth and spread' growth, whereas significantly lower supersaturation conditions were observed at 175 °C and, consequently, crystal growth proceeded through spiral growth. The methodology described in this work could be extended to other zeolitization and/or crystallization processes, provided a homogeneous synthesis mixture and supernatant are available.

Author Contributions

Experimental work and data interpretation were performed by M.H. and E.B, with contributions from M.H., E.V. and S.R. on NMR and K.A. on X-ray diffraction. The project was conceived and supervised by M.W.A., F.T., J.A.M. and C.E.A.K. The manuscript was written through contributions of all authors. All authors have given approval to the final version of the manuscript. The authors declare no competing financial interest.

Acknowledgements

M.H. and E.B. acknowledges FWO for an FWO-SB fellowship and a 'Krediet aan navorsers' 1.5.061.18N. M.H. extends his gratitude to Sara Lieben and Adam Hill for their supervision during his master thesis. J.A.M. and C.E.A.K. acknowledge the Flemish Government for long-term structural funding (Methusalem), the Research Foundation Flanders (FWO) and the Belgian government for Interuniversity Attraction Poles (IAP). NMR equipment was acquired with financial support by Hercules Foundation (AKUL/13/21), and by the Flemish Government, department EWI via the Hermes Fund (AH.2016.134).

Appendix A. Supplementary data

Notes and references

§ Chemical composition: $(K,Na)_5$ $(Ba,Ca)_2$ $[Al_9Si_{23}O_{64}]$. 24 H2O;[20] crystal structure is orthorhombic (space group *Immm*, No. 71) with a = 14.116 Å, b = 14.229 Å and c = 9.946 Å [18, 23]. §§ Pore dimensions vary with orientation: [100] = 3.1 x 3.5 Å, [010] = 2.7 x 3.6 Å and [001] = 3.4 x 5.1 Å and 3.3 x 3.3 Å [35].

[1] J. Grand, H. Awala, S. Mintova, Mechanism of zeolites crystal growth: new findings and open questions, CrystEngComm, 18 (2016) 650-664.

[2] C. Baerlocher, L.B. McCusker, Database of Zeolite Structures, 2013.

[3] N.A. Anurova, V.A. Blatov, G.D. Ilyushin, D.M. Proserpio, Natural Tilings for Zeolite-Type Frameworks, The Journal of Physical Chemistry C, 114 (2010) 10160-10170.

[4] P. Cubillas, M.W. Anderson, M.P. Attfield, Materials Discovery and Crystal Growth of Zeolite A Type Zeolitic–Imidazolate Frameworks Revealed by Atomic Force Microscopy, Chemistry – A European Journal, 19 (2013) 8236-8243.

[5] L.I. Meza, M.W. Anderson, J.R. Agger, Differentiating fundamental structural units during the dissolution of zeolite A, Chem Commun, (2007) 2473-2475.

[6] R. Brent, M.W. Anderson, Fundamental crystal growth mechanism in zeolite L revealed by atomic force microscopy, Angewandte Chemie (International ed. in English), 47 (2008) 5327-5330.

[7] M.W. Anderson, J.T. Gebbie-Rayet, A.R. Hill, N. Farida, M.P. Attfield, P. Cubillas, V.A. Blatov, D.M. Proserpio, D. Akporiaye, B. Arstad, J.D. Gale, Predicting crystal growth via a unified kinetic three-dimensional partition model, Nature, 544 (2017) 456-459.

[8] M. Haouas, L. Lakiss, C. Martineau, J. El Fallah, V. Valtchev, F. Taulelle, Silicate ionic liquid synthesis of zeolite merlinoite: Crystal size control from crystalline nanoaggregates to micron-sized single-crystals, Microporous and Mesoporous Materials, 198 (2014) 35-44.

[9] L. van Tendeloo, M. Haouas, J.A. Martens, C.E. Kirschhock, E. Breynaert, F. Taulelle, Zeolite synthesis in hydrated silicate ionic liquids, Faraday Discuss, 179 (2015) 437-449.

[10] G. Brabants, M. Hubin, E.K. Reichel, B. Jakoby, E. Breynaert, F. Taulelle, J.A. Martens, C.E. Kirschhock, Revisiting Silicalite-1 Nucleation in Clear Solution by Electrochemical Impedance Spectroscopy, Langmuir : the ACS journal of surfaces and colloids, 33 (2017) 2581-2589.

[11] G. Brabants, S. Lieben, E. Breynaert, E.K. Reichel, F. Taulelle, J.A. Martens, B. Jakoby, C.E.A. Kirschhock, Monitoring early zeolite formation via in situ electrochemical impedance spectroscopy, Chemical Communications, 52 (2016) 5478-5481.

[12] A. Aerts, L.R.A. Follens, M. Haouas, T.P. Caremans, M.-A. Delsuc, B. Loppinet, J. Vermant, B. Goderis, F. Taulelle, J.A. Martens, C.E.A. Kirschhock, Combined NMR, SAXS, and DLS Study of Concentrated Clear Solutions Used in Silicalite-1 Zeolite Synthesis, Chemistry of Materials, 19 (2007) 3448-3454.

[13] B. Slater, T. Ohsuna, Z. Liu, O. Terasaki, Insights into the crystal growth mechanisms of zeolites from combined experimental imaging and theoretical studies, Faraday Discussions, 136 (2007) 125.

[14] J. Šefčík, A.V. McCormick, Prediction of crystallization diagrams for synthesis of zeolites, Chemical Engineering Science, 54 (1999) 3513-3519.

[15] V. Nikolakis, D.G. Vlacho, M. Tsapatsis, Modeling of zeolite crystallization: the role of gel microstructure, Microporous and Mesoporous Materials, 21 (1998) 337-346.

[16] L. Van Tendeloo, E. Gobechiya, E. Breynaert, J.A. Martens, C.E. Kirschhock, Alkaline cations directing the transformation of FAU zeolites into five different framework types, Chem Commun (Camb), 49 (2013) 11737-11739.

[17] L. Van Tendeloo, W. Wangermez, A. Vandekerkhove, T. Willhammar, S. Bals, A. Maes, J.A. Martens, C.E.A. Kirschhock, E. Breynaert, Postsynthetic High-Alumina Zeolite Crystal Engineering in Organic-Free Hyper-Alkaline Media, Chemistry of Materials, 29 (2017) 629-638.

[18] E. Galli, G. Gottardi, D. Pongiluppi, The crystal structure of the zeolite merlinoite, Neues Jahrbuch fur Mineralogie - Monatshefte, (1979) 1-9.

[19] P.A. Barrett, S. Valencia, M.A. Camblor, Synthesis of a merlinoite-type zeolite with an enhanced SiAl ratio via pore filling with tetraethylammonium cations, J. Mater. Chem., 8 (1998) 2263-2268.

[20] E. Passaglia, D. Pongiluppi, R. Rinaldi, Merlinoite, a new mineral of the zeolite group, Neues Jahrbuch fur Mineralogie - Monatshefte, 8 (1977) 355-364.

[21] J.D. Sherman, Identification and characterization of zeolites synthesized in the K2O-Al2O3-SiO2-H2O System, ACS Symp. Ser., 40 (1977) 30.

[22] G. Gottardi, E. Galli, Natural Zeolites, Berlin Heidelberg: Springer-Verlag1985.

[23] A. Bieniok, K. Bornholdt, U. Brendel, W.H. Baur, Synthesis and crystal structure of zeolite W, resembling the mineral merlinoite, J. Mater. Chem., 6 (1996) 271-275.

[24] B.M. Fung, A.K. Khitrin, K. Ermolaev, An Improved Broadband Decoupling Sequence for Liquid Crystals and Solids, Journal of Magnetic Resonance, 142 (2000) 97-101.

[25] P. Cubillas, M.W. Anderson, Synthesis Mechanism: Crystal Growth and Nucleation, Zeolites and Catalysis: Synthesis, Reactions and Applications, WILEY-VCH Verlag GmbH & Co., Weinheim, 2010, pp. 1-56.

[26] L.N. Rashkovich, J.J. De Yoreo, C.A. Orme, A.A. Chernov, In situ atomic force microscopy of layer-by-layer crystal growth and key growth concepts, Crystallography Reports, 51 (2006) 1063-1074.

[27] I. Sunagawa, Growth and Morphology of Crystals, Forma, 14 (1999) 147-166.

[28] J.W. Mullin, Crystallization (Fourth Edition), Butterworth-Heinemann, Oxford, 2001.

[29] T.J.W. De Bruijn, W.A. De Jong, P.J. Van Den Berg, Kinetic parameters in Avrami—Erofeev type reactions from isothermal and non-isothermal experiments, Thermochimica Acta, 45 (1981) 315-325.

[30] R.W. Thompson, Nucleation, growth, and seeding in zeolite synthesis, in: H. Robson (Ed.) Verified Synthesis of Zeolitic Materials, Elsevier, Amsterdam, 2001.

[31] W.K. Burton, N. Cabrera, F.C. Frank, The growth of crystals and the equilibrium structure of their surfaces, Phil. Trans. R. Soc. Lond. A, 243 (1951) 299-358.

[32] F.C. Frank, The influence of dislocations on crystal growth, Discussions of the Faraday Society, 5 (1949) 48-54.

[33] T.W. Swaddle, Silicate complexes of aluminum(III) in aqueous systems, Coordination Chemistry Reviews, 219-221 (2001) 665-686.

[34] O. Larlus, V.P. Valtchev, Crystal Morphology Control of LTL-Type Zeolite Crystals, Chemistry of Materials, 16 (2004) 3381-3389.

[35] C. Baerlocher, L.B. McCusker, D.H. Olson, Atlas of Zeolite Framework Types, 6 ed., Amsterdam, 2007.